

Articles

Dual Binding Mode of a Novel Series of DHODH Inhibitors

Roland Baumgartner,* Markus Walloschek, Martin Kralik, Astrid Gotschlich, Stefan Tasler, Jan Mies, and Johann Leban
4SC AG, Am Klopferspitz, 19a, 82152 Martinsried, Germany

Received July 21, 2005

Human dihydroorotate dehydrogenase (DHODH) represents an important target for the treatment of hyperproliferative and inflammatory diseases. In the cell DHODH catalyzes the rate-limiting step of the de novo pyrimidine biosynthesis. DHODH inhibition results in beneficial immunosuppressant and antiproliferative effects in diseases such as rheumatoid arthritis. Here, we present high-resolution X-ray structures of human DHODH in complex with a novel class of low molecular weight compounds that inhibit the enzyme in the nanomolar range. Some compounds showed an interesting dual binding mode within the same cocrystal strongly depending on the nature of chemical substitution. Measured in vitro activity data correlated with the prevailing mode of binding and explained the observed structure–activity relationship. Additionally, the X-ray data confirmed the competitive nature of the inhibitors toward the putative ubiquinone binding site and will guide structure-based design and synthesis of molecules with higher activity.

Introduction

Rheumatoid arthritis (RA) ranks among the top 10 major chronic diseases in western countries. Approximately 1% of the population is affected equating to more than 2 million people in the United States alone. Current treatment of patients usually comprises the use of nonsteroidal antiinflammatory drugs (NSAIDs) as a first-line therapy to relieve pain and inflammation. Second-line treatment involves disease-modifying antirheumatic drugs (DMARDs) like hydroxychloroquine, sulfasalazine, methotrexate, and immunosuppressive agents such as cyclosporine. However, very recently there has been a clear trend toward the use of DMARDs much earlier in the treatment, especially in patients with moderate to severe disease stages. Several excellent reviews surveying existing therapeutic strategies for RA can be found in the literature.¹

The human enzyme dihydroorotate dehydrogenase (DHODH) represents a well-characterized target for small molecular weight DMARDs. Human DHODH belongs to the family class 2 that utilizes flavine as a redox cofactor, unlike the bacterial family class 1 protein that uses fumarate or NAD⁺ instead. In the cell the mammalian protein is anchored at the inner mitochondrial leaflet. There, DHODH catalyzes the conversion of dihydroorotate (DHO) to orotate (ORO), which represents the rate-limiting step in the de novo pyrimidine biosynthesis.² Kinetic studies indicate a sequential ping-pong mechanism for the conversion of DHO to ORO.³ The first half-reaction comprises the reduction of DHO to ORO. Electrons are transferred to the flavine mononucleotide moiety (FMN) which becomes oxidized to dihydroflavin mononucleotide (FMNH₂). After dissociation of ORO from the enzyme, FMNH₂ is regenerated by a ubiquinone molecule, which is recruited from the inner mitochondrial membrane (Figure 1b). Kinetic and structural studies revealed two distinct binding sites for DHO/ORO and ubiquinone, respectively.

Recently, Liu et al.⁴ published the crystal structures of human DHODH in complex with a brequinar analogue (**1**) and an active

metabolite of leflunomide (**2**) bound to the postulated ubiquinone binding site, respectively (Figure 1c). In general, inhibitors of DHODH show beneficial immunosuppressive and antiproliferative activities, most pronounced on T-cells.⁵ Brequinar and leflunomide are two examples of small molecular weight inhibitors of DHODH that had been in clinical development. The latter is used in the treatment of rheumatoid arthritis refractive to methotrexate.^{6,7} Clinical application of both molecules suffers from various side effects. On the basis of very good efficacy in animal models, brequinar was originally developed for the therapy of organ transplant rejection but moved to cancer as a secondary indication. The compound failed in clinic due to its narrow therapeutic window.⁶ Oral administration of brequinar and some of its analogues resulted in toxic effects, including leukocytopenia and thrombocytopenia, when given in combination with cyclosporine.⁷ The application of leflunomide might be flawed by its long half-life time of approximately 2 weeks which represents a serious obstacle in patients that have developed side effects.^{8,9}

Here, we present crystallographic data of our own efforts in developing small molecule inhibitors against human DHODH. We describe an interesting case of a dual binding mode observed for a series of structurally related compounds. Depending on the pattern of chemical substituents, the molecules can be triggered to display either a high-affinity or a low-affinity binding mode or even both at the same time in one cocrystal. The X-ray data confirmed the competitive nature of the inhibitors toward the putative ubiquinone binding site and will facilitate further structure-based design and synthesis of effective small molecules.

Results

We have developed a novel series of DHODH inhibitors, based on virtual screening methods and medicinal chemistry exploration. Initially, docking of a library of commercially available compounds, using our proprietary virtual high-throughput docking method ProPose,^{10,11} yielded some hits with a pharmacophore reminding of, but significantly different from,

* Corresponding author. Phone: (+49) 89 7007 630. Fax: (+49) 89 7007 6329. E-mail: baumgartner@4sc.com.

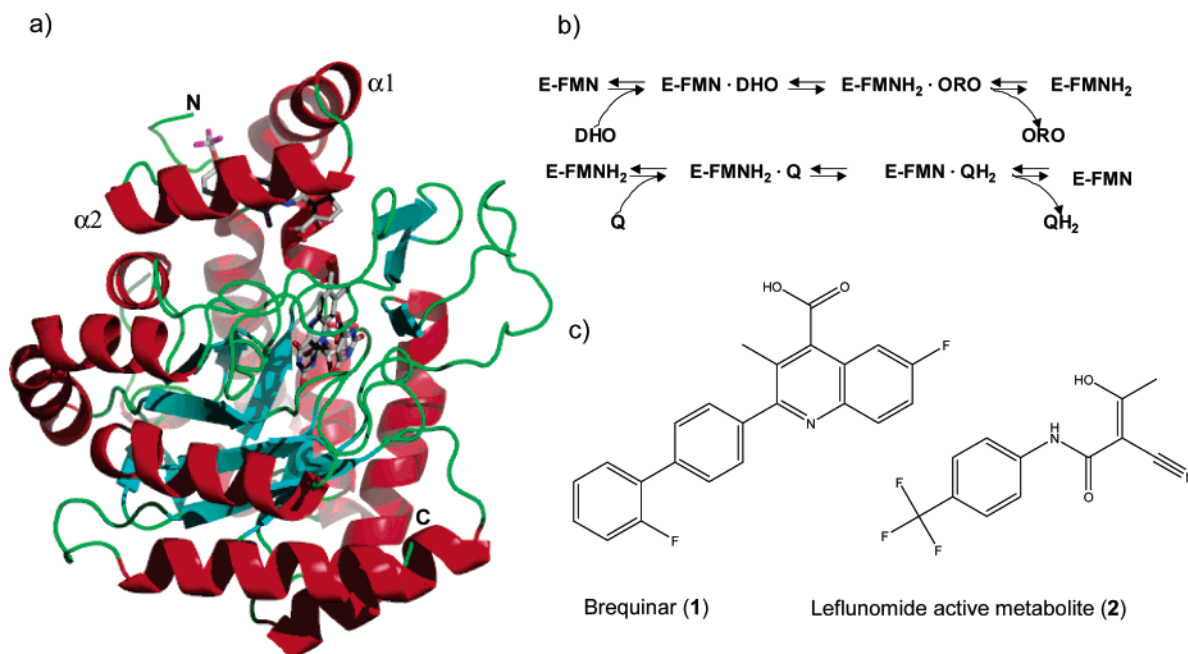
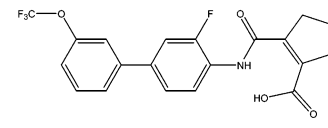
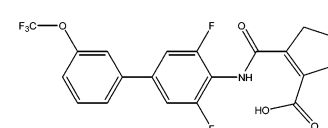
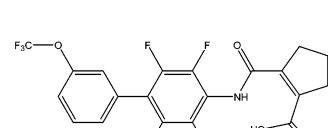
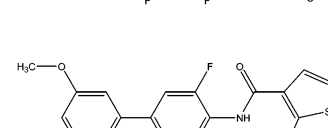
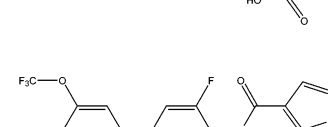


Figure 1. (a) Ribbon diagram showing the overall structure of human DHODH in complex with compound 3. The inhibitor molecule (stick representation) binds in the cleft between the N-terminal helices $\alpha 1$ and $\alpha 2$. The cofactor FMN and one molecule of orotate are depicted in the center. This figure was created with Pymol (ref 33). (b) Scheme of the reaction catalyzed by DHODH. (c) Two known DHODH inhibitors, brequinar (1) and the active metabolite of leflunomide (2).

Table 1. Correlation of Binding Modes, Designated “Brequinar-like” and “Nonbrequinar-like”, with in Vitro Activity Data

Cpd.	Chemical Formula	IC ₅₀	Brequinar-like	Non-Brequinar-like
<u>3</u>		280 nM		X
<u>4</u>		33 nM	X	X
<u>5</u>		7 nM	X	X
<u>6</u>		44 nM	X	X
<u>7</u>		2 nM	X	

brequinar. In essence, these compounds were cyclic aliphatic or aromatic dicarboxylic acids, in which one carboxyl group is amide-bound to an aromatic biphenyl aniline (Table 1). Cheminformatics, chemical synthesis, and hit validation using in vitro and cell-based assays are described elsewhere.¹² To further explore the structural requirements for the design of an “optimal”

DHODH inhibitor, several molecules that displayed structure–activity relationship in an in vitro assay with IC₅₀ values typically between 280 and 2 nM, were selected and cocrystallized with human DHODH (Table 1).

Overall Structure. Human DHODH is composed of two domains, a large C-terminal domain (Met78–Arg396) and a

Table 2

	compound 3	compound 4	compound 5	compound 6	compound 7
(a) Data Collection Statistics					
A. crystal data					
space group	<i>P</i> 3 ₂ 21	<i>P</i> 3 ₂ 21	<i>P</i> 3 ₂ 21	<i>P</i> 3 ₂ 21	<i>P</i> 3 ₂ 21
cell dimensions (Å)	90.6/90.6/123.2	90.6/90.6/123.0	90.4/90.4/123.0	90.7/90.7/122.8	90.3/90.3/122.7
molecules/AU ^d	1	1	1	1	1
resolution (Å)	2.15	2.4	1.95	1.8	2.0
B. data collection					
X-ray source	DESY BW6	DESY BW6	DESY BW6	DESY BW6	DESY BW6
wavelength (Å)	1.05	1.05	1.05	1.05	1.05
total/unique reflections	124056/32175	101935/22253	142628/42908	326335/54728	103711/39080
completeness (%) ^b	99.2/99.0	95.8/97.1	99.8/99.9	99.9/100.0	98.6/99.0
<i>I</i> / σ ^b	14.7/5.7	14.6/3.8	12.6/3.4	27.4/6.0	14.1/3.8
<i>R</i> _{merge} (%) ^{b,c}	7.1/24.8	9.1/38.1	8.2/38.3	6.0/30.6	6.5/24.8
(b) Refinement Statistics					
<i>R</i> -factor (%) ^d	20.1/19.1	17.6/19.4	18.5/20.6	19.5/20.5	18.1/19.7
<i>R</i> _{free} ^e	22.1/23.2	21.1/23.2	20.2/23.6	20.5/22.7	20.0/22.0
rms deviation from ideal					
bond length (Å)	0.005	0.005	0.005	0.005	0.005
bond angles (deg)	1.2	1.2	1.2	1.2	1.2
dihedral angles (deg)	21.5	21.3	21.2	21.9	21.2
improper angles (deg)	0.8	0.81	0.81	0.82	0.8
non-hydrogen atoms (protein)	2778	2778	2770	2784	2784
water molecules	153	250	264	227	291
FMN/ORO/INH ^f	1/1/1	1/1/1	1/1/1	1/1/1	1/1/1
acetate/sulfate	1/2	1/4	3/2	2/4	1/4

^a AU, asymmetric unit. ^b The second value refers to the highest resolution shell. ^c $R_{\text{merge}} = \sum |I - \langle I \rangle| / \sum I$, where *I* is the observed intensity of a reflection and $\langle I \rangle$ is the average intensity obtained from multiple observations of symmetry-related reflections. ^d The second value refers to the highest resolution shell. *R*-factor (working set) = $\sum |F_o| - |F_c| / \sum |F_o|$, where *F*_o and *F*_c are the observed and calculated structure factors, respectively. ^e *R*_{free} (test set), identical to *R*-factor, but calculated for 5% of the reflections omitted from the refinement for cross validation. ^f Flavinmononucleotide (FMN); orotate (ORO); inhibitor molecule (INH).

smaller N-terminal domain (Met30–Leu68), connected by an extended loop. The large C-terminal domain can be best described as an α/β -barrel fold with a central barrel of eight parallel β strands surrounded by eight α helices. The redox site, formed by the substrate binding pocket and the site that binds the cofactor flavin mononucleotide (FMN), is located on this large C-terminal domain. The small N-terminal domain, on the other hand, consists of two α helices (labeled $\alpha 1$ and $\alpha 2$), both connected by a short loop (Figure 1a). This small N-terminal domain harbors the binding site for the cofactor ubiquinone. The helices $\alpha 1$ and $\alpha 2$ span a slot of about $10 \times 20 \text{ \AA}^2$ in the so-called hydrophobic patch, with the short $\alpha 1$ – $\alpha 2$ loop at the narrow end of that slot. The slot forms the entrance to a tunnel that ends at the FMN cavity nearby the $\alpha 1$ – $\alpha 2$ loop. This tunnel narrows toward the proximal redox site and ends with several charged or polar side chains (Gln47, Tyr356, Thr360, and Arg136).

To date, there is no structural information on the binding site of ubiquinone in human DHODH. Structural clues, as discussed above, along with kinetic studies suggest that ubiquinone, which can easily diffuse into the mitochondrial inner membrane, uses this tunnel to approach the FMN cofactor for the redox reaction.

So far, we have solved five structures in complex with low molecular weight compounds. Generally, all structural models are of high-resolution quality with very good stereochemical geometries (see the Experimental Section and Table 2). The data provide clear and excellent electron densities for the inhibitor compounds and therefore enable a detailed analysis of the prevailing interactions and modes of binding.

Nevertheless, some parts of the protein, mainly solvent-exposed loops, appear to be disordered. In particular, residues 69–71 in all structures and residues 216–221 in some of the structures display only poor electron density. The His-tag preceding the N-terminal Met30 is disordered in all structures. Three cis-peptide bonds, starting at residues Gly119, Pro131,

and Val282 can be found in the C-terminal domain; the latter two cis-peptide bonds are supposed to be necessary for FMN binding.⁴

Additionally, the analysis of the solved complex structures clearly indicates a considerable degree of protein flexibility at the N-terminal ubiquinone/inhibitor binding pocket and of residues located in the larger C-terminal domain also involved in inhibitor binding. As will be discussed in some detail below, the protein can accommodate quite a diverse range of ring substitutions as well as two different positions of the carboxy group attached to the five-membered ring.

Binding Mode of Brequinar. The crystal structures of human DHODH in complex with a brequinar analogue and the leflunomide metabolite A77172 were published recently.⁴ As a reference we also solved the crystal structure of human DHODH in complex with brequinar. Structural differences between the two crystal structures are negligible. Both brequinar and its analogue are located in the proposed ubiquinone binding channel. From a structural point of view, there are two major contributions to binding, one predominantly polar and the other predominantly hydrophobic. First, the 6-fluoro-3-methyl-4-quinoline carboxylic acid forms an almost perfectly oriented salt bridge to the side chain of Arg136. Additionally, hydrogen bonds form between the carboxylic acid and the side chain of Gln47 (Figure 2). Second, the biphenyl ring system shows several hydrophobic contacts with residues Leu42, Met43, Leu46, Ala55, Phe58, Leu62, Leu68, Phe98, and Leu359 (Figure 2). The distribution of the amino acids forming the binding site is quite clearly cut into two parts. The entrance of the binding tunnel almost exclusively consists of hydrophobic amino acids. This agrees with the fact that helices $\alpha 1$ and $\alpha 2$ are involved in membrane association. The narrow end of the tunnel forms a rather polar environment capped by a small hydrophobic pocket formed by side chains of Val134 and Val143. Thus, potential ligands should match the amphipathic character of the

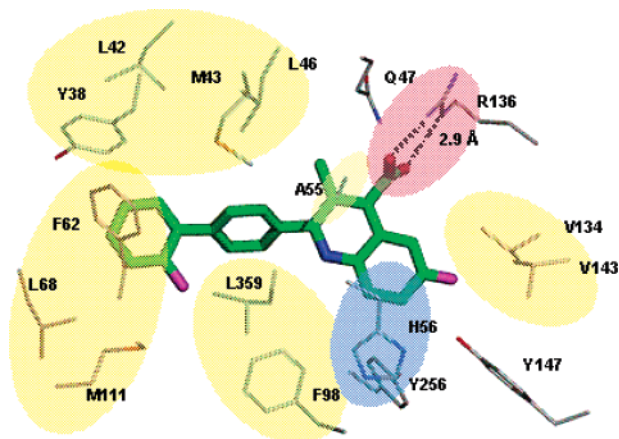


Figure 2. Binding mode of brequinar. Residues contributing to the binding site are shown in stick representation and are labeled with a one-letter code and sequence number. Residues accounting for hydrophobic interactions are shaded in yellow, aromatic stacking in blue, and electrostatic in red. This figure was created with Pymol (ref 33).

inhibitor binding site. Obviously, brequinar and its analogues fulfill this requirement nearly perfectly and therefore exhibit IC_{50} values of around 7 nM in *in vitro* enzyme assays.

Binding Mode of Compound 3. Solving the crystal structure of DHODH in complex with compound **3** was straightforward following the protocol of Liu et al.⁴ The model was refined to a resolution of 2.15 Å with excellent electron density. Originally, it was intended that the carboxy group at the five-membered ring should interact with the side chain of Arg136, thus mimicking a brequinar-like binding mode. Analysis of the compound **3** complex revealed a rather unexpected binding mode. In contrast to the brequinar binding mode, the carboxy moiety is positioned in the opposite direction protruding toward the protein's interior. This binding mode will be termed "nonbrequinar-like" in the following. As a representative example, Figure 3a shows the final Fo–Fc electron density map, calculated with compound **3** omitted, at 2.15 Å resolution. A final refined model of the inhibitor is built into the electron density. The electron density unequivocally reveals that the carboxyl moiety at the five-membered ring protrudes into the

protein's interior and interacts with residues Tyr356 and Tyr147 by the formation of hydrogen bonds. The hydrogen bond to Tyr356 is formed directly, whereas the hydrogen bond to Tyr147 is mediated by a water molecule (Figure 3b). The five-membered ring is located in a plane with the adjacent amide bond. Probably an intramolecular hydrogen bond between the amide and the carbonyl oxygen of the carboxy moiety is formed.

Interestingly, in this structure Arg136 displays two well-resolved side chain conformations. For both conformations the *b*-factors of the side chain atoms are not significantly above the mean value (mean, 22.5 Å²; Arg136—extended, 25.6 Å²; Arg136—solvent exposed, 26.1 Å²). One conformation displays an extended side chain that covers the top of the binding site, whereas in the second conformation the side chain protrudes away into the solvent region.

The electron density for Gln47 is less straightforward to interpret and must be discussed in the context of the Arg136 conformations. In Figure 4 two pairs of compatible side chain conformations of Gln47 and Arg136 are shown. When the side chain of Arg136 is pointing away from the binding site toward the solution (grey-coded conformation in Figure 3b), Gln47 can be modeled into a well-resolved electron density. If Arg136 is built in the more extended conformation (red side chain in Figure 3b), there would be a sterical clash with Gln47. To avoid this, the side chain of Gln47 would have to be rotated toward the solvent region. There is no electron density visible for interpretation in this area, and thus Gln47 is replaced by alanine in Figure 3b.

For residue His56, Liu et al. proposed that the imidazole ring of His56 stacks with the fluoroquinoline ring of brequinar. Contrastingly, in our crystal structures the imidazole ring is rotated away by almost 70° from its "brequinar-like" position toward the carboxy group of the inhibitor molecule. The imidazole ring can be placed either with the ND1 atom or the CD1 atom toward the inhibitor. Since a water molecule on the opposite side of the imidazole ring is within hydrogen-bonding distance to ND1 (distance 2.6 Å), the latter orientation might be correct. Furthermore, by rotating the imidazole ring in the opposite orientation the distance between ND1 and the inhibi-

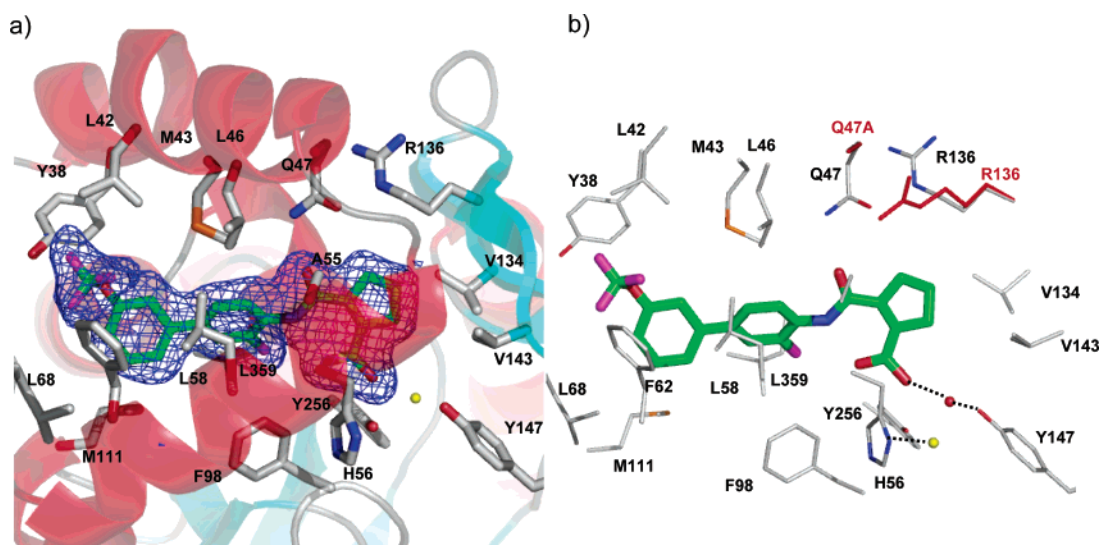


Figure 3. Mode of binding of compound **3**. (a) Close-up of the binding site. Important residues are presented as sticks and are labeled with a one-letter code and sequence number. An Fo–Fc electron density, contoured at 3σ , is shown for the inhibitor. (b) Same orientation and labeling as in (a); water molecules are shown as colored spheres (red and yellow), hydrogen bonding is indicated by dashed lines. Residues Q47 and R136 are shown in an alternative conformation in red. Q47 is built as alanine, labeled Q47A, due to missing electron density. The figures were created with Pymol (ref 33).

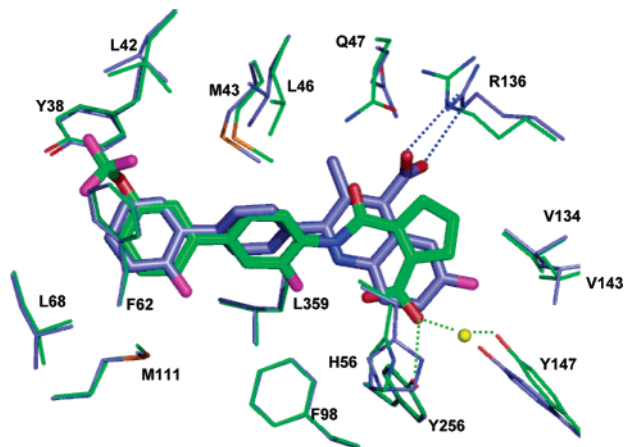


Figure 4. Superposition of the DHODH inhibitor binding site complexed with **3** (green color code) and the DHODH inhibitor binding site complexed with brequinar (**1**) (blue color code). Side chain residues are labeled with a one-letter code and sequence number; residues A55 and L62 are not shown. A water molecule, mediating a hydrogen bond between **3** and Y147, is drawn as a yellow sphere. Important polar interactions are depicted as dashed lines marked in the respective color code. The carboxy group of **1** forms a salt bridge with residue R136. Compound **3** exhibits its main polar interactions with Y356 and Y147, thus binding in a “nonbrequinar-like” manner with respect to the carboxyl group. The figures were created with Pymol (ref 33).

tor’s carboxy group exceeds 3 Å and a hydrogen-bond interaction can be ruled out.

Finally, the biphenyl ring system occupies most of the hydrophobic pocket in a manner similar to that of brequinar. The two aromatic rings are inclined to each other by approximately 70°, a value closely resembling that of brequinar. The quinoline moiety of **1** and the cyclopentene ring of **3** are located almost exactly in the same plane. Figure 4 shows a

superposition of brequinar and compound **3**, demonstrating the almost opposite modes of interaction of the respective carboxy groups.

Binding Mode of Compounds 4 and 5. Upon investigating the electron density maps for compounds **4** and **5** we found that the density covering the five-membered ring appears more extended and less detailed than one would expect at a resolution of 1.95 and 2.4 Å, respectively (Figure 5a). Residual density in the Fo–Fc electron density map indicates missing model input (Figure 5b). The electron density appears big enough to accommodate the compounds in an alternative conformation where the five-membered ring is rotated by 180°, probably around the biphenyl/amide bond, thus indicating the presence of a “brequinar-like” binding mode. The carboxy group and the carbonyl oxygen perfectly fit into the residual density of the Fo–Fc map (Figure 5c). Moreover, after refinement and map calculation with the compounds in “brequinar-like” conformation, the residual density reappears at positions corresponding to the “nonbrequinar-like” binding mode.

Interestingly, in the structures of compounds **4** and **5** the side chains of both Gln47 and Arg136 display a unique conformation similar to the one found in the brequinar structure. Electron densities are well-defined for both residues, signs of a second conformation are observed neither in the Fo–Fc electron density map nor in an omit-map calculated for this amino acid positions. The water molecule bridging the hydrogen bond between the carboxy group and Tyr147 is present in both structures. Residue His56 adopts the same conformation as observed in the complex with **3**. Alterations in the conformation of the biphenyl ring system in comparison to compound **3** were not observed. A comparison of the binding sites of compound **3** with compound **5** is shown in Figure 6. The binding sites superpose with an rmsd of 0.18 Å. Besides conformational differences of Gln47 and Arg136, as discussed above, there are only marginal variations among the two binding modes. These observations

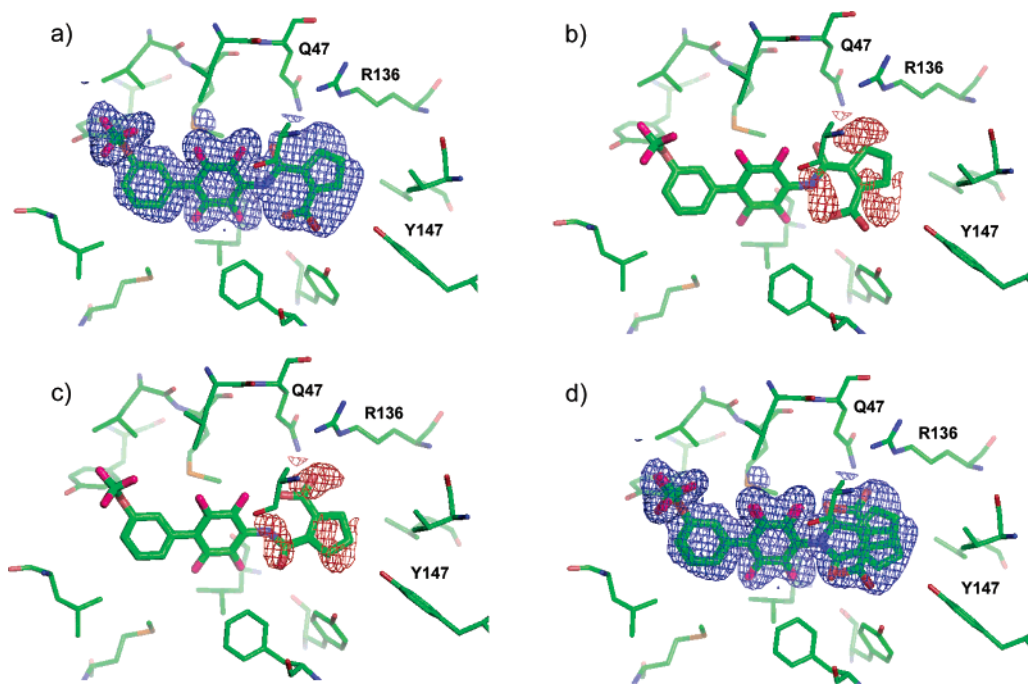


Figure 5. Analysis of the mode of binding of compound **5**. (a) Final Fo–Fc (blue) electron density, calculated with compound **5** omitted, contoured at 3 σ . (b) Fo–Fc map (red), calculated in the presence of compound **5** in nonbrequinar-like conformation, contoured at 3 σ . (c) Same electron density map as in (b), but with the five-membered ring rotated at the biphenyl amide bond. (d) Same electron density as in (a); now two models of compound **5**, one in brequinar-like and one in nonbrequinar-like conformation, are built in the electron density. The figures were created with Pymol (ref 33).

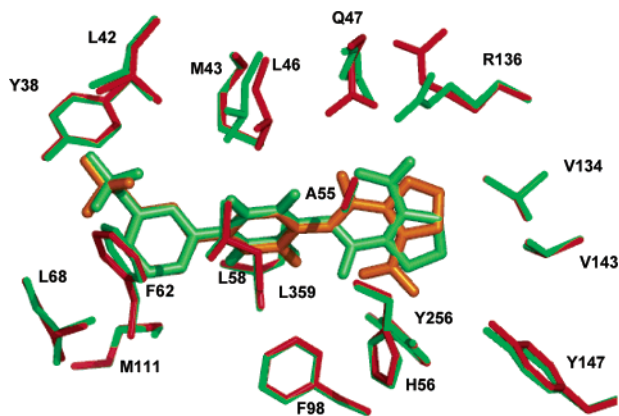


Figure 6. Superposition of the binding sites of compound **3** (red) and compound **5** (green). Compound **3** represents the “nonbrequinar-like” binding mode with the carboxy group protruding to the protein’s interior. Compound **5** is shown in the “brequinar-like” conformation where the carboxy group interacts with residues Arg136 and Gln57. The figures were created with Pymol (ref 33).

suggest that the binding sites of **4** and **5** constitute a conformational superposition of both binding modes which might be occupied with equal fractions within one cocrystal.

Binding Mode of Compounds 6 and 7. These compounds mainly differ from compounds **4** and **5** by the replacement of the cyclopentene ring for a thiophene ring. The crystal structures were solved at 1.8 Å resolution for compound **6** and at 2.0 Å resolution for compound **7**. Inspection of the electron density revealed a mixed-type binding mode, very similar to that of compounds **4** and **5**, for compound **6** (Figure 7a), whereas in the structure of compound **7** a “brequinar-like” mode of binding is the only occupied conformation (Figure 7b). Residues Gln47 and Arg136 display a unique conformation in both structures. The water molecule bridging the hydrogen bond between the carboxy group and Tyr147 is present in **6** but missing in the structure of **7**. The pattern of interactions is not significantly different from that found in the complex structures of **4** and **5**. However, the sulfur atom of the thiophene is in close contact to a small hydrophobic pocket formed by the side chains of Val134 and Val143 thus contributing an additional interaction to the binding affinity that is not present in the other molecules.

The solved complex structures enable a more detailed characterization of the structural properties of inhibitor binding

site. According to the specific nature of the protein ligand interactions one can identify a number of subsites. It is instructive to assume a kind of “unified” or “maximal” inhibitor molecule, obtained by a superposition of the prevailing binding modes (Figure 8) and serving as a probe for the identification of interaction centers. Each subsite includes molecular functional groups capable of forming stabilizing interactions with complementary functional groups of a possible inhibitor molecule. The major part of the binding site is made up by the hydrophobic subsite 1, which is adequately occupied by the biphenyl rings. Subsites 2 and 3 can be addressed by functional groups capable of forming hydrogen bonds. In the present cases this is realized by the carboxy group attached to the cyclopentene ring and by the ability to form a dual binding mode. Finally, the binding pocket is capped by a more remote hydrophobic site (subsite 4). Inhibitors **6** and **7** utilize subsite 4 for hydrophobic interaction via the sulfur of the thiophene ring. We propose a fifth subsite for binding, predominately polar in nature, consisting of the hydroxy group of Tyr38 and the backbone carbonyl of Leu62. This subsite is in close proximity to the $-\text{OCF}_3$ or $-\text{OCH}_3$ groups attached in meta position to the second ring of the biphenyl system. Although we do not observe interactions by these groups, it appears reasonable to design future inhibitors containing functional groups which anchor the inhibitor molecules at subsite 5.

The biological activity data indicated a correlation of binding affinities with compound structure. The closer an inhibitor molecule matches the subsites the higher the affinity for the enzyme. Specifically, the “brequinar-like” binding mode exhibits higher affinity than the “nonbrequinar-like” mode. Often this cannot be easily explained by just making up the balance of observed, mainly polar, interactions since one cannot account for the hydrophobic contribution properly (see discussion below). Nevertheless, the dissection of the fine structure of the binding site might serve as a blueprint for even more active compounds. For instance, one could visualize a molecule carrying two functional groups at the five-membered ring in order to address both subsites 2 and 3 simultaneously.

Discussion

In our attempt to better understand the structure–activity relationship of a novel series of DHODH inhibitors several cocrystal structures have been solved at high resolution. Surprisingly, within this class, some of the compounds showed

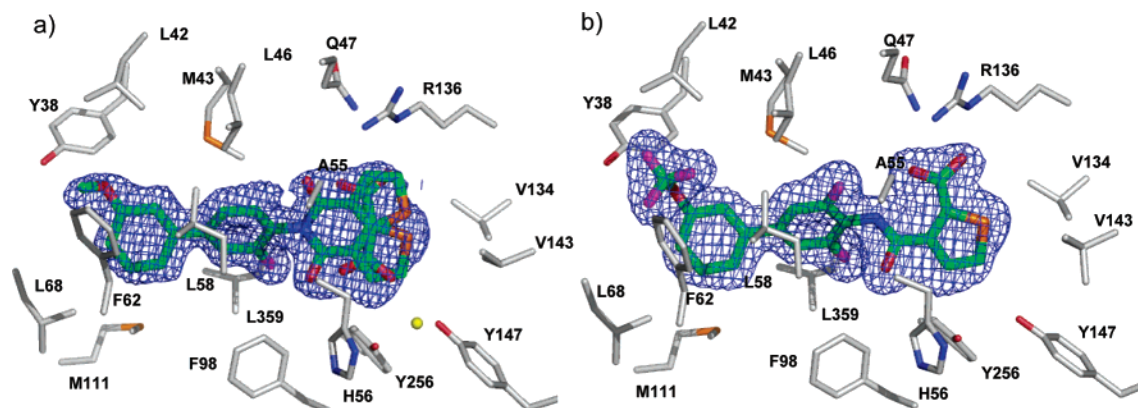


Figure 7. (a) Detail of the DHODH inhibitor binding site complexed with compound **6**. The final Fo–Fc (blue) electron density, calculated with compound **6** omitted, is contoured at 3σ . Two molecules of **6** are built into the density, one in a “brequinar-like” conformation (carboxyl group position in the upward direction) and one in a “nonbrequinar-like” conformation (carboxyl group position in the downward direction). Side chain residues are labeled with a one-letter code and sequence number; a water molecule is depicted as a yellow sphere. (b) Drawing of compound **7** bound into the DHODH inhibitor binding site. The molecule displays a 100% “brequinar-like” conformation. Side chain residues are labeled with a one-letter code and sequence number; the water molecule is missing. The figures were created with Pymol (ref 33).

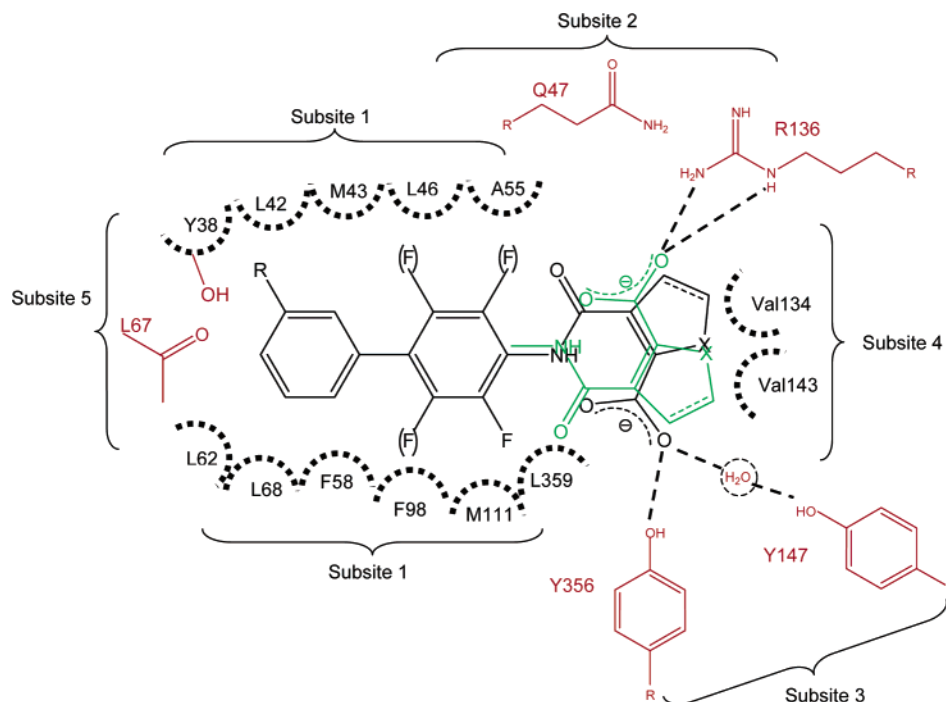


Figure 8. Schematic diagram of the DHODH inhibitor binding site representing several subsites, labeled 1–5, suitable for interacting with an inhibitor molecule. Black dotted circles depict residues contributing to hydrophobic interactions; amino acids contributing to electrostatic interactions are highlighted in red. The drawing of the inhibitor molecule represents a “consensus” molecule, with differing degrees of fluorine substitution, indicated by (F), a variable substituent R ($R = -OCF_3$ or $-OCH_3$), and a heteroatom X ($X = S$) at the five-membered ring. The alternative conformation of the inhibitor is depicted in green. Possible hydrogen bonding is indicated by black dashed lines; amino acids are given in a one-letter code plus sequence number.

a dual binding mode. The two alternative conformations were designated “brequinar-like” and “nonbrequinar-like”, respectively. In the “brequinar-like” binding mode the compounds adopt a conformation where the carboxy group of the five-membered ring forms hydrogen bonds with the side chains of residues Gln47 and Arg136. In the “nonbrequinar-like” binding mode the five-membered ring is rotated by almost 180° and forms hydrogen bonds with residues Tyr356 and, mediated by a water molecule, with residue Tyr147. The side chain conformations of Gln47 and Arg136 are not uniquely defined in the case of full “nonbrequinar-like” binding, whereas for mixed-type and full “brequinar-like” binders Arg136 always adopts a unique conformation and the side chain of Gln47 is well ordered. Very recently, crystal structures of the rat DHODH (DHODR) in complex with brequinar and atovaquone were published.¹³ The authors report a key role for Arg136 in the interaction with electron acceptors of the inhibitor molecules. Similar to our results, the side chain of Arg136 displays adaptive flexibility in order to achieve an optimal alignment toward electron-accepting groups of the inhibitor molecules.

A superposition of binding sites accommodating either a “brequinar-like” binder or a “nonbrequinar-like” binder reveals conformational differences for residues Gln47 and Arg136, whereas for the rest of the binding pocket conformational differences are only marginal (Figure 6). On the other hand, the binding site displays sufficient volume to accommodate a variety of ring substitutions and compound conformations, especially for the hydrophobic part of the binding site. Probably, the modulation of the respective binding modes is mainly influenced by the chemical nature of the compounds themselves. Compounds **3**, **4**, and **5** are particularly interesting for a structure–activity relationship (SAR) analysis. These molecules differ only in the degree of ring substitution (Table 1). All three compounds adopt a similar conformation in the binding pocket.

The two aromatic rings of the central biphenyl system are inclined to each other by approximately $120\text{--}135^\circ$. In none of the compounds is the trifluoromethoxy group located in the plane of the adjacent phenyl ring but forms a C–C–O–CF₃ dihedral angle of 75° (**3**), 85° (**4**), and 91° (**5**). The $-OCF_3$ group might act as an anchor group in its hydrophobic environment made up by residues Tyr38 and Leu42. This agrees with the findings of Böhm et al.¹⁴ who investigated the values of the C–C–O–CF₃ dihedral angles in trifluoromethoxybenzenes without substituents in ortho positions. Five out of six entries in the Cambridge Structural Database (CSD) displayed values of around 90° .

Significant differences can be observed at the position of the carboxyl group attached to the cyclopentene ring, as discussed above. The degree of fluoro substitution in the adjacent aromatic ring seems a crucial factor in modulating the respective binding modes. Fluorine as a substituent in organic molecules is known to enhance lipophilicity,¹⁴ to change the basicity or acidity,¹⁵ and is able to change the preferred conformation of a molecule due to its size and electronegativity. In the present case the observed increased binding affinity most likely reflects a combination of these effects. Calculated log *P* values (compound **3**, 4.8; compound **4**, 5.0; compound **5**, 5.2; calculated with MOE¹⁶) indicate a slight increase of hydrophobicity along with an increasing number of fluorine substituents. The fluorine substituents in the ortho position might exert a steering effect on the five-membered ring and facilitate the formation of the more favorable “brequinar-like” binding mode. In contrast to these more indirect effects on binding affinity, the role of fluorine in polar interactions is a matter of debate in the literature.^{14,17} Examples where covalently bound fluorine might be engaged in hydrogen bonds in protein–ligand complexes are reported for fluorinated thrombin inhibitors¹⁸ and p38 kinase inhibitors.¹⁴ In these crystal structures C–F...N distances of

3.47 Å and C–F···O=C distances of 3.21 and 4.47 Å were observed, respectively. In our structures distances from the C–F units to potential acceptors or donors are not within the reported ranges. Therefore, contributions from polar interactions can be ruled out.

In compounds **6** and **7**, the cyclopentene ring is replaced by a thiophene ring. Judged by the number of fluorine substituents on the aromatic ring system we anticipated a “nonbrequinar-like” binding mode for compound **6** (one fluorine atom) and a dual binding mode for compound **7** (two fluorine atoms). These predictions were in contrast to the measured in vitro IC₅₀ values. The activity data suggest a dual binding mode for compound **6** (IC₅₀ = 44 nM, Table 1) and a “brequinar-like” behavior for compound **7** (IC₅₀ = 2 nM, Table 1). The solved protein–ligand complexes confirmed the in vitro data since compound **6** was found to exhibit a dual binding mode and compound **7** binds fully “brequinar-like”. The conformations adopted by compound **6** and **7** reveal no significant differences when compared to those of compounds **4** and **5**. However, the sulfur atom of the thiophene ring closely packs to the side chains of Val134 and Val143 (Figure 7) mediating an additional hydrophobic interaction.

We have identified molecules which are able to adopt either the “brequinar-like” binding mode or the “nonbrequinar-like” binding mode or both binding modes within the same crystal structure. The in vitro activity data reflect this differential binding profile of the molecules quite well. The more “brequinar-like” the smaller the measured IC₅₀ values (Table 1), which suggests that the “brequinar-like” binding mode is more favorable.

Examples of dual or even multiple binding modes have been described in the literature. Usually it is observed that a series of compounds with closely related inhibitor scaffolds displays different binding modes in the respective crystal structures.^{19–23} In some cases activity data can be correlated with individual binding modes.¹⁹ Further interesting cases report the same ligand molecule in a forward orientation in one crystal structure and in a backward orientation in a second crystal structure.²⁴ Wojtczak et al. present the crystal structure of tetrameric rat transthyretin which possesses two unique hormone binding sites. The data revealed the natural ligand thyroxine oriented differently in the two binding sites.²⁵ However, the example presented here is different as there is a dual binding mode of the inhibitor molecule addressing alternative binding sites of the protein at the same time in one cocrystal structure. Frequently, a predominantly hydrophobic binding site is observed in cases of multiple binding modes. Besides the important factor of substituent effects the rather unspecific nature of the hydrophobic interaction may also be required to enable multiple inhibitor binding modes. On the other hand, predominantly lipophilic binding pockets constitute serious conceptual problems for docking algorithms. Attempts reported in the literature to reproduce the crystal structure for DHODH in complex with brequinar were successful but failed in the case of leflunomide.²⁶ In our own docking attempts, using the proprietary software ProPose,^{10,11} we found that the molecules reflect the X-ray data sufficiently well, although the dual binding modes cannot be reproduced. Care should be taken in implementing scoring functions that take into account the binding site characteristics.^{27,28}

To summarize, these results have important implications for SAR predictions of compounds as the measured activity is a result of the sum of the binding constant of both (or multiple) binding modes. The use of computational tools such as docking

and virtual screening should involve extensive structural studies in order to derive useful models.

Experimental Section

In Vitro Enzyme Assay. The standard assay mixture contained 50 μM decyclo-ubiquinone, 100 μM dihydroorotate, and 60 μM 2,6-dichloroindophenol (DCIP). The amount of enzyme was adjusted such that an average slope of approximately 0.2 AU/min will be achieved in the assay for the positive control (e.g., without inhibitor). Measurements were conducted in 50 mM TrisHCl, 150 mM KCl, 0.1% Triton X-100, pH 8.0, at 30 °C in a final volume of 1 mL. The components were mixed, and the reaction was started by adding dihydroorotate. The reaction was followed spectrophotometrically by measuring the decrease in absorption at 600 nm for 2 min. The assay was linear in time and enzyme concentration. Inhibitory studies were conducted in a standard assay with additional variable amounts of inhibitor. For the determination of the IC₅₀ values (concentration of inhibitor required for 50% inhibition) eight different inhibitor concentrations were applied. Each data point was recorded in triplicates on a single measurement day. Data were analyzed with the program GraFit³⁴ using a four-parameter fit.

Crystallization. Human DHODH (Met30-Arg396) was expressed and purified as described by Liu et al.⁴ Cocrystallization trials with 4SCs inhibitors and brequinar at 20 °C were performed using the hanging-drop vapor diffusion method. Drops were formed by mixing equal amounts of 20 mg/mL protein in 50 mM HEPES, pH 7.7, 400 mM NaCl, 30% glycerol, 1 mM EDTA, and 10 mM *N,N*-dimethylundecylamin-*N*-oxide (C11DAO) with a precipitant solution of 0.1 M acetate pH 4.6–5.0, 40 mM C11DAO, 20.8 mM *N,N*-dimethyldecylamine-*N*-oxide (DDAO), 2 mM dihydroorotate (DHO), 1.8–2.4 M ammonium sulfate, and 1 mM compound. The drops were incubated against 0.5 mL of reservoir of 0.1 M acetate pH 4.8, 2.4–2.6 M ammonium sulfate and 30% glycerol. Crystals usually appeared as small cubes within 3 days and reached a full size of 0.2 × 0.2 × 0.2 mm³ within 3–4 weeks. The protein crystallized in the space group *P*₃21. For data collection crystals were flash frozen directly in the cryo stream.

Data Collection and Phasing. Data were collected at beam line BW6 at the DESY, Hamburg, on a MAR-CCD camera. The crystals were maintained at a temperature of 100 K during data collection. The indexing and integration of the reflection intensities was performed with the program MOSFLM.²⁹ Data were scaled and merged with SCALA²⁹ and reduced to structure factor amplitudes with TRUNCATE.²⁹ Data collection statistics are shown in Table 1. The structures for human DHODH (Met30–Arg396) inhibitor complexes were solved using molecular replacement (MR). The pdb entry 1D3G.pdb, without ligands and water molecules, was used as a search model. A standard rotational and translational molecular replacement search, usually between 3 and 3.5 Å, was performed using the program MOLREP.²⁹ In all cases the solutions for both the rotational and translational search were well above the next ranking solutions. The MR resulted in *R*-factors typically around 35% and a correlation coefficient of > 60%. Correct packing of symmetry-related molecules was checked visually in O.³⁰

Refinement and Model Building. For refinement of the initial model resulting from the molecular replacement hit, the program CNX³¹ and the CCP4²⁹ suite were used. Model building and electron density manipulations were carried out using the O program,³⁰ coordinate files for the inhibitors were created with the program MOE.¹⁶ In a first round of refinement the MR model was subjected to rigid body refinement followed by a slow-cooling simulated-annealing protocol using a maximum likelihood target to remove model bias. Additionally, an individual *b*-factor refinement was carried out using standard CNX protocols. Finally, SIGMAA-weighted 2Fo–Fc and Fo–Fc electron density maps were calculated and displayed together with the protein model in the program O. In later refinement cycles a conventional minimization procedure based on a maximum likelihood target was used. Finally, water picking was done using CNX. A pdb file for each inhibitor compound was created using the program MOE. After energy

minimization the compound was built into the electron density manually. Topology and parameter files for each compound were created using the program Xplo2d.³² Refinement was considered to have converged when $R_{\text{free}} < 25\%$ was reached. Usually the final models include the polypeptide representing human DHODH (Met30–Arg396), the cofactor flavine mononucleotide (FMN), one orotate molecule (ORO), several acetate molecules (ACT), sulfate ions (SO₄), one molecule of inhibitor (INH), and water molecules (TIP or WAT, respectively). Statistics of refinement are given in Table 2. For benchmarking purpose the crystal structure of DHODH in complex with brequinar (**1**) was solved according to the procedure described in ref 4. The dataset has a resolution of 1.9 Å and is 98.5% complete. The final refined model exhibits an R -factor and R_{free} of 19.1% and 21.3%, respectively. The coordinates of the complexes (compounds **3–7**) will be deposited at the Protein Data Bank (pdb entry code, 2BXV, 2FPT, 2FQI, 2FPV, 2FPY).

Acknowledgment. We thank Matthias Dormeyer, Bernd Kramer, Sylvia Lemstra, and Stefan Strobl for useful discussions and Daniel Vitt and Gerhard Keilhauer for their support. We also thank BW6 beam line staff, DESY Hamburg, for excellent support.

References

- (1) (a) Smolen, J. S.; Steiner, G. Therapeutic strategies for rheumatoid arthritis. *Nat. Drug Discovery* **2003**, *2*, 473–484. (b) Weinblatt, M. E. Rheumatoid arthritis in 2003: where are we now with treatment? *Ann. Rheum. Dis.* **2003**, *62*, 94–96. (c) Simon, L. S.; Yocum, D. New and future drug therapies for rheumatoid arthritis. *Rheumatology* **2000**, *39* (Suppl.1), 36–42.
- (2) McLean, J. E.; Neidhardt, E. A.; Grossmann, T. H.; Hedstrom, L. Multiple inhibitor analysis of brequinar and leflunomide binding sites on human dihydroorotate dehydrogenase. *Biochemistry* **2001**, *40*, 2194–2200.
- (3) Knecht, W.; Henseling, J.; Löffler, M. Kinetics of inhibition of human and rat dihydroorotate dehydrogenase by atovaquone, lawsone derivatives, brequinar sodium and polyporic acid. *Chem. Biol. Interact.* **2000**, *124*, 61–76.
- (4) Liu, S.; Neidhardt, E. A.; Grossman, T. H.; Ocain, T.; Clardy, J. Structure of human dihydroorotate dehydrogenase in complex with antiproliferative agents. *Structure* **2000**, *8*, 25–33.
- (5) Fairbanks, D.; Bofill, M.; Ruckemann, K.; Simmonds, H. A. Importance of ribonucleotide availability to proliferating T-lymphocytes from healthy humans. Disproportionate expansion of pyrimidine pools and contrasting effects of de novo synthesis inhibitors. *J. Biol. Chem.* **1995**, *270*, 29682–29689.
- (6) Rozman, B. Clinical experience with leflunomide in rheumatoid arthritis. *J. Rheumatol. Suppl.* **1998**, *53*, 27–31.
- (7) Pally, C.; Smith, D.; Jaffe, B.; Magolda, R.; Zehender, H.; Dorobek, B.; Donatsch, P.; Papageorgiou, C.; Schurman, H.-J. Side effects of brequinar and brequinar analogues, in combination with cyclosporine, in the rat. *Toxicology* **1998**, *127*, 207–222.
- (8) Fox, R. I. Mechanism of action of leflunomide in rheumatoid arthritis. *J. Rheumatol. Suppl.* **1998**, *53*, 20–26.
- (9) Alldred, A.; Emery, P. Leflunomide: A novel DMARD for the treatment of rheumatoid arthritis. *Expert Opin. Pharmacother.* **2001**, *2*, 125–137.
- (10) Seifert, M. H.; Schmitt, F.; Herz, T.; Kramer, B. ProPose: A docking engine based on a fully configurable protein–ligand interaction model. *J. Mol. Model.* **2004**, *10*, 342–357.
- (11) Seifert, M. H. ProPose: steered virtual screening by simultaneous protein–ligand docking and ligand–ligand alignment. *J. Chem. Inf. Model.* **2005**, *45*, 449–460.
- (12) Leban, J.; Saeb, W.; Garcia, G.; Baumgartner, R.; Kramer, B. Discovery of a novel series of DHODH inhibitors by a docking procedure and QSAR refinement. *Bioorg. Med. Chem. Lett.* **2004**, *14*, 55–58.
- (13) Hansen, M.; LeNours, J.; Johansson, T. A.; Ullrich, A.; Löffler, M.; Larsen, S. Inhibitor binding in a class 2 dihydroorotate dehydrogenase causes variations in the membrane-associated N-terminal domain. *Protein Sci.* **2004**, *13*, 1031–1042.
- (14) Böhm, H.-J.; Banner, D.; Bendels, S.; Kansy, M.; Kuhn, B.; Müller, K.; Obst-Sander, U.; Stahl, M. Fluorine in medicinal chemistry. *ChemBioChem* **2004**, *5*, 637–643.
- (15) van Niel, M. B.; Collins, I.; Beer, M. S.; Broughton, H. B.; Cheng, S. K.; Goodacre, S. C.; Heald, A.; Locker, K. L.; MacLeod, A. M.; Morrison, D.; Moyes, C. R.; O'Connor, D.; Pike, A.; Rowley, M.; Russell, M. G.; Sohal, B.; Stanton, J. A.; Thomas, S.; Verrier, H.; Watt, A. P.; Castro, J. L. Fluorination of 3-(3-(piperidin-1-yl)propyl)indoles and 3-(3-(piperazin-1-yl)propyl)indoles gives selective human 5-HT_{1D} receptor ligands with improved pharmacokinetic profiles. *J. Med. Chem.* **1999**, *42*, 2087–2104.
- (16) MOE 2002.02.; Chemical Computing Group Inc.: Montreal, Canada, 2002.
- (17) Dunitz, J. D. Organic fluorine: Odd man out. *ChemBioChem* **2004**, *5*, 614–621.
- (18) Olsen, J. A.; Banner, W.; Seiler, P.; Obst-Sander, U.; D'Arcy, A.; Stihle, M.; Müller, K.; Diederich, F. A fluorine scan of thrombin inhibitors to map the fluorophilicity/fluorophobicity of an enzyme active site: evidence for C–F···C=O interactions. *Angew. Chem., Int. Ed.* **2003**, *42*, 2507–2511.
- (19) Lange, G.; Lesuisse, D.; Deprez, P.; Schoot, B.; Loenze, P.; Bernard, D.; Marquette, J.-P.; Broto, P.; Sarubbi, E.; Mandine, E. Principles governing the binding of a class of nonpeptidic inhibitors to the SH2 domain of src studied by X-ray analysis. *J. Med. Chem.* **2002**, *45*, 2915–2922.
- (20) Llorens, O.; Perez, J. J.; Palomer, A.; Mauleon, D. Differential binding mode of diverse cyclooxygenase inhibitors. *J. Mol. Graphics Modell.* **2002**, *20*, 359–371.
- (21) Holtz, K. M.; Stec, B.; Myers, J. K.; Antonelli, S. M.; Widlanski, T. S.; Kantrowitz, E. R. Alternate modes of binding in two crystal structures of alkaline phosphatase-inhibitor complexes. *Protein Sci.* **2000**, *9*, 907–915.
- (22) Lewis, P. J.; Jonge, M.; Daeyaert, F.; Koymans, L.; Vinkers, M.; Heeres, J.; Janssen, P. A. J.; Arnold, E.; Das, K.; Clark, A. D., Jr.; Hughes, S. H.; Boyer, P. L.; Bethune, M.-P.; Pauwels, R.; Andries, K.; Kikla, M.; Ludovici, D.; DeCorte, B.; Kavash, R.; Ho, C. On the detection of multiple-binding modes of ligands to proteins, from biological, structural, and modeling data. *J. Comput.-Aided Mol. Des.* **2003**, *17*, 129–134.
- (23) Poulos, T. L.; Howard, A. J. Crystal structures of metyrapone- and phenylimidazole-inhibited complexes of cytochrome P-450cam. *Biochemistry* **1987**, *26*, 8165–8174.
- (24) Ytterhoeven, K.; Sponer, J.; Van Meerwelt, L. Two 1: 1 binding modes for distamycin in the minor groove of d(GGCCAATTGG). *Eur. J. Biochem.* **2002**, *269*, 2868–2877.
- (25) Wojtczak, A.; Cody, V.; Luft, J. R.; Pangborn, W. Structure of rat transthyretin (rTTR) complex with thyroxine at 2.5 Å resolution: first nonbiased insight into thyroxine binding reveals different hormone orientation in two binding sites. *Acta Crystallogr., Sect. D* **2001**, *57*, 1061–1070.
- (26) Pospisil, P.; Kuoni, T.; Scapozza, L.; Folkers, G. Methodology and problems of protein–ligand docking: case study of dihydroorotate dehydrogenase, thymidine kinase, and phosphodiesterase 4. *J. Recept. Signal Transduction Res.* **2002**, *22*, 141–154.
- (27) Schulz-Gasch, T.; Stahl, M. Binding site characteristics in structure-based virtual screening: evaluation of current docking tools. *J. Mol. Model.* **2003**, *9*, 47–57.
- (28) Erickson, J. A.; Jalaie, M.; Roberston, D. H.; Lewis, R. A.; Vieth, M. Lessons in molecular recognition: the effects of ligand and protein flexibility on molecular docking accuracy. *J. Med. Chem.* **2004**, *47*, 45–55.
- (29) Collaborative Computational Project, N. The CCP4 suite: Programs for protein crystallography. *Acta Crystallogr., Sect. D* **1994**, *50*, 760–763.
- (30) Jones, T. A.; Zou, J.-Y.; Cowan, S. W.; Kjeldgaard, M. Improved methods for building protein models in electron density maps and the location of errors in these models. *Acta Crystallogr., Sect. A* **1991**, *47*, 110–119.
- (31) Brunger, A. T.; Adams, P. D.; Clore, G. M.; DeLano, W. L.; Gros, P.; Grosse-Kunstleve, R. W.; Jiang, J. S.; Kuszewski, J.; Nilges, M.; Pannu, N. S.; Read, R. J.; Rice, L. M.; Simonson, T.; Warren, G. L. Crystallography & NMR system: A new software suite for macromolecular structure determination. *Acta Crystallogr., Sect. D* **1998**, *55*, 905–921.
- (32) Kleywegt, G. J. Validation of protein models from C-alpha coordinates alone. *J. Mol. Biol.* **1997**, *273*, 371–376.
- (33) DeLano, W. L. *The PyMOL Molecular Graphics System 2000*; DeLano Scientific: San Carlos, CA, 2000.
- (34) Leatherbarrow, R. J. *Grafit*, version 5, Erithacus Software Ltd.: Horley, U.K., 2001.